Bottom-Up Synthesis and Top-Down Organisation of Semiconductor and Metal Clusters on Surfaces

Alexander M. Bittner,*[a] Xiao C. Wu,[a,b] Sinan Balci,[a] Mato Knez,[a,c] Anan Kadri,[d] and Klaus Kern[a]

Keywords: Cadmium sulfide / Nanocrystals / Metal clusters / Microcontact printing / Nanostructures / Template synthesis

Near-spherical dendrimers can be used as templates for bottom-up syntheses of semiconductor clusters. Starting from methanolic solutions of Cd^{2+}, sulfide, and poly(amidoamine) dendrimers, CdS clusters precipitate at the dendrimers. A preparation inside the dendrimers is only possible when the protonation of the latter is carefully controlled. The clusters have diameters above about 2 nm and show blue photoluminescence. The patterning and orientation of CdS/dendrimer clusters on flat surfaces are attained by microcontact printing. Depending on the ripening of the CdS/dendrimer suspension, a sub-micrometer stripe pattern develops inside the micrometer-scaled patterns; it extends over the complete surface. Rod-like plant virions with a different type of lateral organisation can be oriented on a flat substrate by applying mechanical forces during immobilisation from suspensions. These virions can also be employed as templates, in this case for creating metal structures by electroless deposition (chemical metal deposition). The structures are wire-like with diameters of 3–4 nm and are confined inside the central channel of the virions. The early stage of the metallisation process is analysed, and a model that accounts for the selectivity is presented.

Introduction

The synthesis of well-defined clusters can be carried out by wet chemical means (under mild conditions) when the products are bound to a template. a range of organic templates, for example block copolymers[1] and biotemplates,[2,3] some of which are single molecules, are available for various semiconductor and metal clusters. The template can direct their size and shape, and it can even catalyse the growth. Typical examples are amphiphiles, which may organise into micelles by self-assembly.[1,4] The clusters are more or less strongly bound to the template, which can be removed to liberate pure clusters.[5] However, in many cases (e.g. for optical measurements) this removal is neither required nor an advantage, such as for photoluminescing CdS clusters at dendrimers.[6,7] The physical properties depend mainly on the cluster size and nature. Thus, while metal clusters reach the limit of quantised conductivity only for very small diameters (<2 nm), even relatively large semiconductor clusters (tens of nanometres) show quantised energy levels, which is reflected in their optical properties, especially photoluminescence.[8]

Nanoscale science and nanotechnology rely, in many cases, on the step-by-step assembly of nano-objects on substrate surfaces. An important issue is how to immobilise and orient the objects at defined sites of a given substrate. Considering that the simplest "bottom-up" syntheses for nano-objects employ molecular templates, soft matter manipulation might be important. On the other hand, standard photo- or electron-beam lithography is slow, expensive and often not compatible with soft matter. Hence, new "top-down" methods are called for, and microcontact printing has been developed into one of the most powerful tools in this respect. Recently, very large molecules such as DNA[9] and inorganic nanowires[10] have been shown to be printable.

Dendrimers are branched macromolecules, and the number of branches determines their generation (here eight terminal branches for generation 1, and 16 for generation 2) and hence their size. In contrast to most polymers, dendrimers have an extremely sharp size distribution. They have been used as templates for spherical clusters of metals and semiconductors;[11–17] cluster diameters are usually below 5 nm. Large rod- or tube-like biological molecules and supramolecular aggregates qualify as templates for quasi-one-dimensional nanostructures. They can be well defined in their chemical composition and also in their structure and symmetry. Examples are DNA,[18] plant virions,[19] phages,[20] protein tubes[21,22] and protein fibres,[23,24] all of

[a] Max-Planck-Institut für Festkörperforschung,
Heisenbergstr. 1, 70569 Stuttgart, Germany
Fax: +49-711-689-1079
E-mail: a.bittner@fkf.mpg.de
[b] New address: National Center for Nanoscience and Technology,
Beijing, China
[c] New address: Max-Planck-Institut für Mikrostrukturphysik,
Halle, Germany
[d] Biologisches Institut, Universität Stuttgart,
Pfaffenwaldring 57, 70550 Stuttgart, Germany

 DOI: 10.1002/ejic.200500388

which are increasingly used for nanoscale structuring as functional units or as templates.[18–29] Apart from binding organic molecules, the best-known templating function is binding (or synthesis) of metal clusters and wires, as presented here for the tobacco mosaic virus (TMV).

As mentioned above, possible applications of semiconductor and metal clusters require a transfer to a substrate surface on a selected area in a defined orientation. For templated clusters, it is sufficient to transfer and orient the template as this results automatically in transfer/orientation of the clusters. The transfer method can be by adsorption, although microcontact printing offers selective placement in predefined arrays. Moreover, in certain cases − here aged CdS/dendrimer composites − the printing process results in sub-patterns that develop inside the printed patterns, and hence structuring on two length scales can be achieved in a single step. For many applications, however, the orientation of nonspherical nano-objects, for example in a parallel fashion, is more important than their exact placement. For this, a range of relatively simple methods is available. For example, laterally (parallel to the substrate surface) applied forces that act on a droplet of suspended nano-objects are well known for stretching and orienting DNA;[9,29,30] here they were tested for the orientation of virions.

The theme of this paper is the combination of "top-down" methods for orientation and placement of nano-objects with their "bottom-up" synthesis. Section 1 introduces a new pH-controlled synthesis method for CdS clusters inside poly(amidoamine) (PAMAM) dendrimer templates. The diameter of the clusters is so small that the energy levels are shifted, hence UV-excited photoluminescence is observed in the blue range of the spectrum. CdS/dendrimer composites can be patterned by microcontact printing. This method can, for certain composites, result in "patterned patterns", i.e. in structures with linear substructures. Section 2 is dedicated to linear structures only; it introduces two very simple orientation methods for TMV, namely blow-drying of a droplet, and exerting capillary forces on a droplet by suction with a filter paper. Both methods have been widely applied, but have not been documented in detail for TMV. The virions can be advantageously employed as templates for 3–4-nm-wide metal wires that are confined in the central channel of the virion; the focus is here on the initial stages of the electroless metal deposition process, and on the surprisingly high selectivity for the inner channel of TMV.

Results and Discussions

1. Synthesis and Organisation of Luminescent CdS Clusters in Micrometer and Sub-Micrometer Patterns

The simple and effective one-pot synthesis of CdS clusters from Cd^{2+} and S^{2-} at dendrimers is well documented.[6,7,15–17] When amine-based dendrimers are employed, their protonation has a pronounced effect on the shape, number and location of the formed nanocrystals. Good examples are near-spherical, amine-terminated PAMAM [poly(amidoamine)] dendrimers of generations 4 ($G4NH_2$) and 8 ($G8NH_2$), where the repeat unit is $N–(CH_2CH_2–CONH–CH_2CH_2)_2$ and the terminal groups are primary amines (NH_2). The Cd^{2+} ions appear to bind to the terminal amine groups, thus usually placing the clusters on the surface of the dendrimers rather than inside. However, Section 1.1 shows that a better control of morphology and size can be obtained by careful protonation of some of the amine groups, which has been discussed for poly(propylene imine) (PPI) dendrimers[31] but has not yet been applied for the synthesis of CdS. The use of hydroxy-terminated dendrimers (G4OH) is an interesting and viable alternative since Cd^{2+} binds only weakly to hydroxy groups.

The "bottom-up" synthesis at a template can be complemented by a "top-down" method to organise the dendrimer/CdS composites in a predefined pattern. Microcontact printing is especially attractive due to its speed, simple handling and variability.[7] Pure semiconductor clusters are difficult to print, so a two-step technique is usually employed: first, a thin layer or monolayer of an organic molecule is printed on a flat substrate to achieve a pattern with chemical contrast, for example hydrophilic/hydrophobic. The clusters are thereafter deposited on the structured susbstrate. A much simpler one-step process, in which the complete dendrimer/CdS composite is printed, could therefore be advantageous.[7] In this way, micrometer-sized areas can be selectively and densely covered with CdS clusters. However, the printing density depends on the age of the CdS/dendrimer suspension. Long ageing times (many days) are preferred due to an improvement of the optical quality. Section 1.2 presents and discusses a new organisation phenomenon that operates with composites aged for only two days: the formation of sub-micrometer line patterns inside the patterned areas.

1.1. Synthesis of CdS Clusters at and in Dendrimer Templates

Balogh et al. have defined three different types of metal–dendrimer nanocomposites according to the position of the metal nanoparticles on the dendrimers,[32] namely metal nanoparticles residing inside the dendrimers (internal type), outside the dendrimers (external type) and a mixed type. The formation of the different types is determined by the binding mechanism of the metal ions (which are synthetic precursors for the clusters), by immobilisation reactions, and by metal–dendrimer interactions during the formation of the nanoparticles. The same principle is employed for semiconductor clusters. According to the actual size of the synthesised nanoparticles (D_N), the diameter of the dendrimers (D_D) and the size of the nanoparticles calculated from the number of metal ions bound to each dendrimer (D_C), the constitution of the nanocomposites can be deduced. Thus, when D_N is smaller than both D_D and D_C, several nanoparticles are found per dendrimer. This occurs for large dendrimers (high generation numbers).[33] Here dendrimers can be called "nanoreactors", as nanoparticles are protected by dendrimer "ligands". However, the size of the nanoparticles cannot be simply estimated from the loading

factor of metal ions to the dendrimer. For example, stable colloidal solutions of CdS/G8NH_2 can be obtained only at NH_2/Cd^{2+} ratios lower than 2 (without control of pH). This indicates that the nucleation sites of the CdS nanoparticles are close to the terminal NH_2 groups. Therefore, CdS clusters are most probably found at the surface regions of the dendrimers, i.e., CdS nanoparticles are (weakly) bound to the terminal NH_2 groups. The diameter (D_N) of the CdS nanoparticles, calculated from the absorption band gap,[34] is about 2 nm,[6] which is smaller than the values of 9.7 and 3.4 nm calculated for D_D and D_C, respectively. Thus, the CdS/G8NH_2 nanocomposites reported by Wu et al.[6,7] belong to the external type, and consist of about two nanoparticles per dendrimer.

When D_N is similar to D_C, one nanoparticle should form per dendrimer. This is the case when the interactions between metal ions and internal functional groups of dendrimers are strong,[35,36] or when the loading of metal ions is confined inside the dendrimers.[15] In this case, the nucleation and also the growth of a nanoparticle is confined within a single dendrimer. The size of nanoparticles can be controlled by the loading factor of metal ions to dendrimers or by the variation of the dendrimer generation. While this is well known for metal/dendrimer composites, semiconductor/dendrimer composites require a more careful control of the protonation.[15] NH_2-Terminated dendrimers undergo various stages of protonation/deprotonation processes at different pH values.[31,37] Therefore, if one can control the protonation of the dendrimers, i.e., only protonate the terminal NH_2 groups and keep the tertiary N groups deprotonated, the CdS clusters should be confined inside the dendrimers. After the synthesis, the NH_3^+ groups can be deprotonated and further chemical modifications can be carried out. Another advantage is that aggregation effects should be reduced due to the repulsive interaction between protonated dendrimers.

1.1.1. pH-Dependent Behaviour of PAMAM Dendrimers

In order to distinguish the protonation processes of tertiary and primary N, various amounts of acid were added to dendrimer (+ Cd^{2+} + S^{2-}) solutions, and conventional pH measurements were carried out. Such measurements are difficult in methanol, but the effects of protonation on the absorption spectra are easily detectable and can be used qualitatively to elucidate the chemical behaviour of the dendrimers. An advantage of the spectroscopic method employed here is that disadvantageous measurement conditions, such as high electrolyte concentration and water as solvent, which are required for accurate pH measurements, can be avoided.

Figure 1 shows the evolution of the absorption spectra of G4OH and G4NH_2 dendrimers in aqueous solution as a function of added amounts of aqueous HCl. G4OH is terminated by OH groups and can therefore not be protonated at its termini, at least in the range of pH values employed. With increasing H^+/NR_3 ratio, the oscillator strength of the C–N bonds (both $\sigma\rightarrow\sigma^*$ and $n\rightarrow\sigma^*$ bonds) in G4OH obviously decreases at first. This can be seen clearly from the variations of absorbance of these two bands with the H^+/NR_3 ratio (see parts a and b in Figure 1) and can be divided into two stages: the rapidly decreasing stage corresponds to the protonation of tertiary N in G4OH, while the flat stage indicates the completion of the protonation process. G4NH_2 (Figure 1, parts c and d) is slightly different to G4OH as it shows a three-stage behaviour. First, the absorption spectra show a small red-shift, and the variation in absorbance is small. After this stage, the changes are similar to those found with G4OH, therefore the first stage should correspond to the protonation of primary N. Note that the changes in the spectra caused by adding HCl can be recovered by adding NaOH. This verifies that the changes are caused by reversible protonation processes.

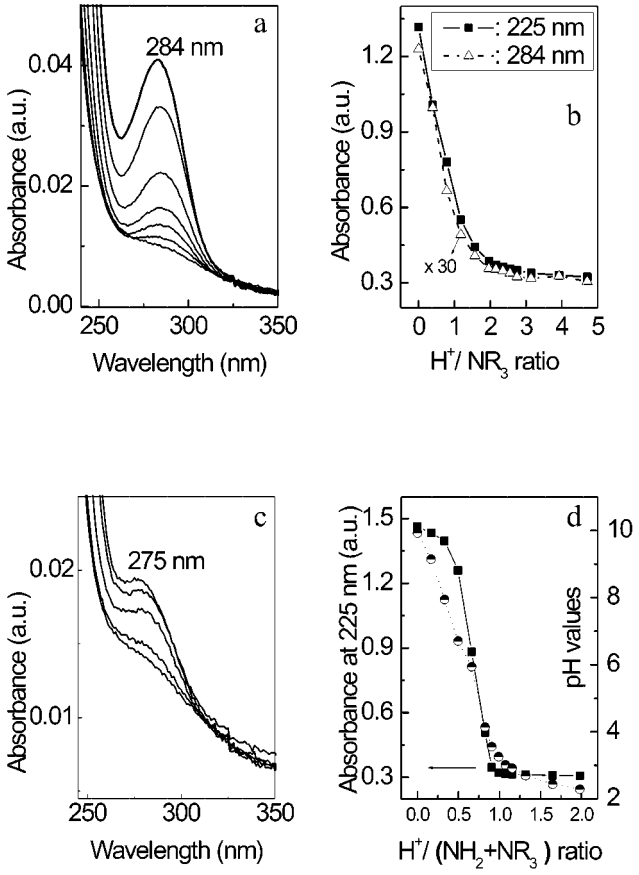

Figure 1. Evolution of absorption spectra of G4OH in aqueous solution, $H^+/(NH_2 + NR_3)$ ratios from top to bottom: 0, 0.39, 0.79, 1.18, 1.57, 2.36, 4.72 (a). Variations of absorbance at 225 and 284 nm vs. H^+/NR_3 ratios; note that the absorption intensity at 284 nm is scaled by a factor of 30 (b). Evolution of absorption spectra of G4NH_2 in aqueous solution, H^+/NR_3 ratio from top to bottom: 0, 0.66, 0.83, 0.91, 0.99 (c). Variations of absorbance (squares) at 225 nm and of pH values (circles) vs. $H^+/(NH_2 + NR_3)$ ratio (d).

In order to check the correlation between the variations in absorption and in protonation, several aliquots from each sample were taken and used for additional pH measurements. They show a good correlation (Figure 1, d). The position of the pH curve at pH 8 corresponds well to the

turning point of the absorbance at 225 nm [$H^+/(NH_2 + NR_3)$ ratio of 0.3], thus indicating the start of the protonation of the tertiary N. Therefore, the relatively flat part of the curve [H+/(NH_2 + NR_3) ratio 0.3–0.6] can be used to synthesise CdS nanoparticles inside dendrimers: The tertiary amine groups remain deprotonated, thus binding of Cd^{2+} is favoured here.

A good comparison with these results is afforded by the protonation behaviour of poly(propylene imine) (PPI) dendrimers, which has been investigated both experimentally and theoretically.[31] At pH 6–8, PPI dendrimers show the desired protonation behaviour. Compared to PPI dendrimers, NH_2-terminated PAMAM dendrimers possess additional amide groups. Since the protonation of amide groups can be neglected at the pH values discussed here, one can assume that PAMAM dendrimers behave similarly to PPI dendrimers.

These results can be extended to larger dendrimers, namely $G8NH_2$. Figure 2 (a) shows pH values for $G8NH_2$ and $G4NH_2$ plotted against the ratio $H^+/(NH_2 + NR_3)$. The pH values of $G4NH_2$ in 1 M aqueous KCl solution serve as a reference. The pH values for $G8NH_2$ at a low electrolyte concentration with methanol as solvent are similar to those at a high electrolyte concentration with water as solvent. Above pH 5 they overlap well, indicating a similar protonation behaviour. However, methanolic solutions exhibit unstable pH readings and long response times during the experiment, which is well known for non-aqueous systems with low electrolyte concentrations. Figure 2 (b) presents the absorption spectra of CdS/$G8NH_2$ nanocomposites in methanol synthesised at different $H^+/(NH_2 + NR_3)$ ratios. It is known that about two CdS nanoparticles bind per dendrimer at pH 10, which is indicative of at least two final nucleation sites at the surface of the dendrimer. In contrast, at pH 6–7, the CdS particle size increases (compared to the case at pH 10). If Cd^{2+} ions are confined inside the dendrimer, one final nucleation site is preferred. In this case, the CdS cluster size should increase, which was indeed observed. Hence, it is postulated that CdS is encapsulated inside the dendrimer when the synthesis is carried out at pH 6–8. After further decrease of the pH value, precipitates form; for these cases, only the absorption spectrum of the supernatant is shown.

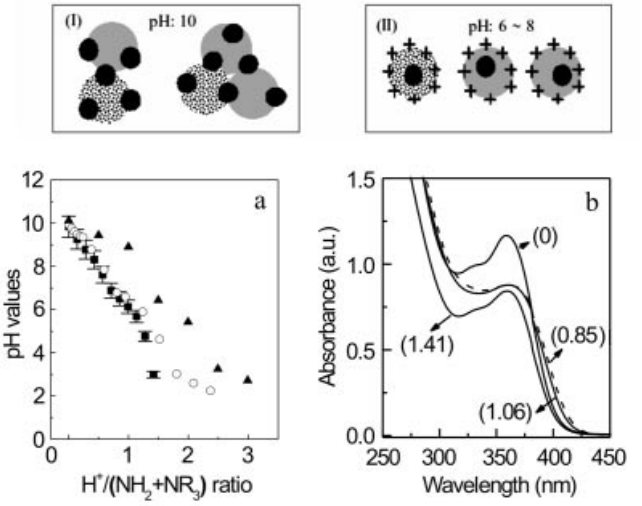

Figure 2. (a) pH values for $G8NH_2$ and $G4NH_2$ at different solvent and electrolyte concentrations vs. ratio $H^+/(NH_2 + NR_3)$. Solid squares: $G8NH_2$ in 0.16 M NaBr in methanol; open squares: $G8NH_2$ in 1 M aqueous NaCl; triangles: $G4NH_2$ in 1 M aqueous NaCl. Upper part (I): Possible morphology of CdS/$G8NH_2$ nanocomposites synthesised at pH 10. (b) Absorption spectra of CdS/$G8NH_2$ nanocomposites in methanol synthesised at selected $H^+/(NH_2 + NR_3)$ ratios; for 1.41 the supernatant was used. Upper part (II): Possible morphology of CdS/$G8NH_2$ nanocomposites synthesised at pH 6–8.

1.1.2. Binding of Cd^{2+} to PAMAM Dendrimers

In the following, syntheses at a pH of around 10 will be discussed for comparison. In these cases, CdS nucleates on

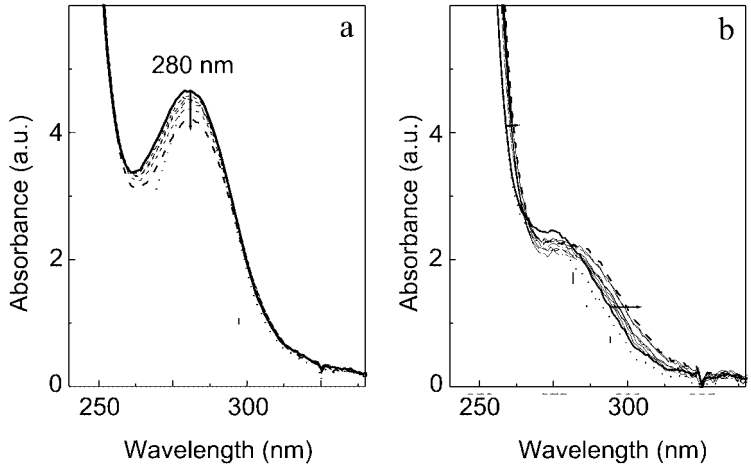

Figure 3. Effects of Cd^{2+} ions on the UV/Vis absorption spectra in methanol: (a) G4OH, ratios Cd^{2+}/NR_3 in direction of arrow (down): 0, 0.2, 0.4, 0.6, 1, 2; bottom spectrum: superposition of absorption spectra of pure G4OH and pure $Cd(CH_3COO)_2$. (b) $G4NH_2$, ratios $Cd^{2+}/(NH_2 + NR_3)$ in direction of arrow (right): 0, 0.08, 0.16, 0.24, 0.32, 0.4, 0.48, 0.64, 0.8; bottom spectrum: superposition of absorption spectra of pure $G4NH_2$ and pure $Cd(CH_3COO)_2$.

the outer dendrimer surface. The interaction strength of N-containing groups with metal ions normally follows the order $-NH_2 > -NR_3 > -CONHR$ (where R is an alkyl chain).[38,39] The example given in Figure 3 shows the effect of Cd^{2+} ions on the UV/Vis absorption spectra of G4OH and $G4NH_2$. The absorption spectrum of pure dendrimers shows two bands that are related to C–N bonds. The strong one around 220 nm results from the $\sigma\rightarrow\sigma^*$ transition of the C–N bonds, while the weak one around 270 nm corresponds to the $n\rightarrow\sigma^*$ transition of the C–N bonds. In order to show the change of the latter, the strong absorption peak of the former is not shown here. The interaction between Cd^{2+} and N-containing groups can be described as a donor–acceptor interaction (lone pair–cation) and is relatively weak. For the Cd^{2+}/G4OH system, the $\sigma\rightarrow\sigma^*$ and $n\rightarrow\sigma^*$ transitions of the C–N bonds show a small decrease in absorbance intensity and no shift of the band. The superposition of the absorption spectra of pure G4OH and pure $Cd(CH_3COO)_2$ with a Cd^{2+}/NR_3 molar ratio of 2:1 is also shown for comparison. It shows a negligible effect. For the Cd^{2+}-$G4NH_2$ system, the $\sigma\rightarrow\sigma^*$ and $n\rightarrow\sigma^*$ transitions of the C–N bonds show a small red-shift, thereby indicating an increased interference by Cd^{2+} ions compared with the case of G4OH. The superposition of the absorption spectra of pure $G4NH_2$ and pure $Cd(CH_3COO)_2$ with a $Cd^{2+}/(NH_2 + NR_3)$ molar ratio of 0.8 shows a small decrease in absorption due to dilution. Since the difference between G4OH and $G4NH_2$ is that $G4NH_2$ has primary amine groups, the interaction of Cd^{2+} with NH_2 groups must be stronger than its interaction with NR_3 groups, which also follows the usual trend in complex chemistry. Obviously, such an interaction favours binding to the outermost chemical groups, hence external type composites are obtained.

1.2. Microcontact Printing of Dendrimers and CdS\|Dendrimer Composites

The "top-down" patterning of flat substrate surfaces with dendrimers is based on interactions like electrostatic forces or hydrogen binding: the larger the dendrimer, the slower its surface diffusion and hence the simpler its selective transfer by microcontact printing. In this case, patterns do not change during and after printing, which is possible for short- and medium-chain thiols on gold.[40,41] First, a dendrimer solution is contacted with the patterned polymer stamp. In most cases the stamp has to be hydrophilic, which for the standard silicone material [poly(dimethylsiloxane)] (PDMS) is achieved with an O_2 plasma treatment. After drying, the stamp is contacted with the (hydrophilic) substrate. One can apply this process also to dendrimer/nanocluster composites because their transfer properties are imposed by the dendrimers, not by the clusters. In other words, the dendrimer functions as an adhesion promoter for "direct" printing. Thus, the usual two-step process, where a chemically functional (or hydrophobic/hydrophilic) pattern has first to be created before adsorbing the clusters or composites, can be avoided.[42] The transferred composite with CdS retains its luminescence properties, and patterning of various micrometre shapes has been demonstrated.[7] As shown in the following, careful variation of the synthesis and printing parameters allows for a better control and even for new organisation phenomena on the substrate surface.

1.2.1. Adsorption of PAMAM Dendrimers

A prerequisite for surface structuring with molecules (or by composites) is adsorption or immobilisation of the molecules. PAMAM dendrimers terminated by NH_2, COOH and OH groups can adsorb on oxides or OH-terminated surfaces via hydrogen bonds.[6,43] Part a of Figure 4 shows an example of the adsorption of G4OH, $G4NH_2$ and $G8NH_2$ dendrimers from solution onto oxidised Si wafers. The adsorption process is very fast and reaches nominal monolayer thickness (see below) for all three dendrimers within several minutes. Further immersion changes the ellipsometric thickness only slightly. Hence, a nominal monolayer is formed. The heights of the G4 and G8 monolayers

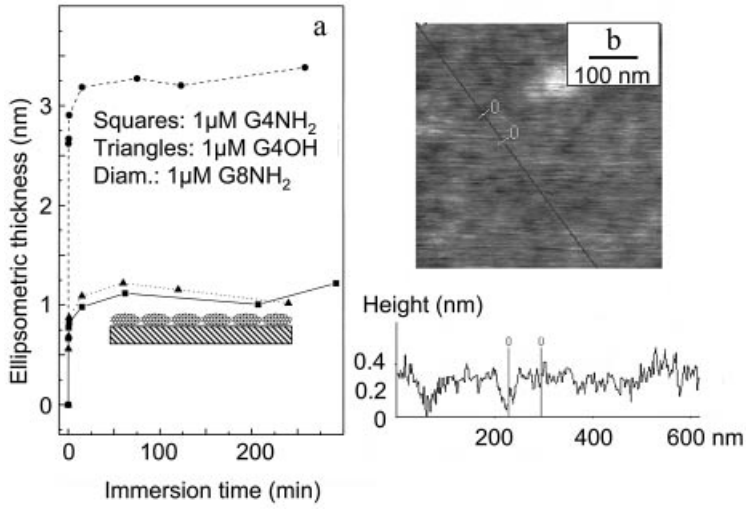

Figure 4. (a) Ellipsometric thickness of G4OH, $G4NH_2$ and $G8NH_2$ on oxidised silicon wafer surfaces measured in air after immersion, rinsing with ethanol and drying with argon. (b) Topographic intermittent contact AFM image of $G4NH_2$ monolayer on an oxidised silicon wafer; bottom part: height profile.

are around 1.2 and 3.3 nm, respectively, which means large deviations from their ideal spherical diameters of 4.5 and 9.7 nm.[44] The monolayer thicknesses are, however, close to the height of single G4 and G8 dendrimers on hydrophilic surfaces.[45] This indicates that a strong interaction with the hydrophilic surfaces deforms the dendrimers and they show an oblate morphology on these surfaces. A topographic AFM image of a $G4NH_2$ monolayer on a wafer is shown in Figure 4 (b). The white dot in the upper part is a defect, probably due to local multiplayer adsorption. Lateral structures were not observed. The image shows hillocks whose height cannot be determined exactly. The hillocks are ascribed to the $G4NH_2$ monolayer, which is quite flat, as can be seen from the height profile (<1 nm variation). Although the tip geometry plays a role in smoothing out the image, holes in the layer more than 5 nm in diameter should be easily visible. One can deduce that the coverage is smooth and dense. Due to this adsorption behaviour, dendrimers can be printed well on hydrophilic surfaces.[46]

1.2.2. Stripe Patterns of CdS/Dendrimer Composites

In the course of the microcontact printing experiments, an interesting new phenomenon of a "bottom-up" organisation inside "top-down" patterned areas was discovered. For this, only composites that have been aged for a short time (two days at ambient temperature in the synthesis solution) qualify, i.e. particles with a monodisperse size distribution (Figure 5, a).[6] For longer ageing times, Ostwald ripening occurs (for this reason the term "ageing" is preferred over "long term synthesis"). This not only increases the size of the CdS nanoparticles but it also changes the morphology of the whole nanocomposites, which is advantageous for the printing.[6] After two days, the average height (measured by AFM) of the nanocomposites is around 9 nm, and they have a regular shape. In contrast, after 22 days the height of the particles varies from 10 nm to 60 nm, and the distributions of both shape and size broaden considerably (Figure 5, b).

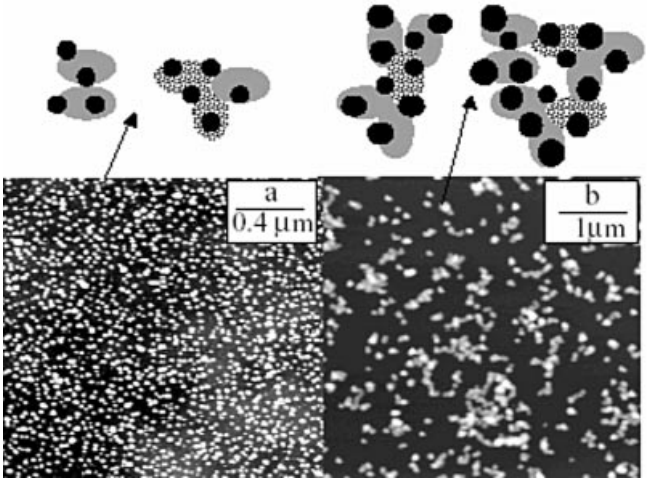

Figure 5. Topographic AFM images of $CdS/G8NH_2$ nanocomposites adsorbed on an oxidised silicon wafer after two days ageing (a) and after 22-days ageing (b). Upper parts: possible morphology for each case.

These relatively large composite aggregates can be organised into predefined micropatterns. First, a PDMS polymer stamp is produced by curing a liquid silicone prepolymer on a patterned silicon master. The patterned stamp is peeled off and treated with an oxygen plasma to create a hydrophilic stamp surface. This surface, in analogy to oxidised silicon wafers (Figure 5), is ideally suited for binding CdS/dendrimer composites aged for 22 d, simply by contacting the solution with the stamp and drying it. Conformal contact with a flat hydrophilic substrate transfers the composites exactly in the predefined pattern.

When the ageing time is reduced to only two days, the distribution of the composites on the substrate does not simply follow the pattern, rather a stripe structure several hundreds of nanometres wide develops inside the pattern, as can be seen in Figure 6. Note that the experiment was carried out in the same way, only the ageing time was shortened. The stripe structure appears to extend over the complete substrate. Hence a sub-micrometer "bottom-up" stripe patterning is obtained by using "top-down" micropatterning (>5 µm width). Height modulations on the stamp surface are not decisive: the same phenomenon occurs with unpatterned (flat) stamps (Figure 7), which are formed on flat, unpatterned silicon wafers. Such flat stamps usually transfer the adsorbed substance uniformly on the substrate.

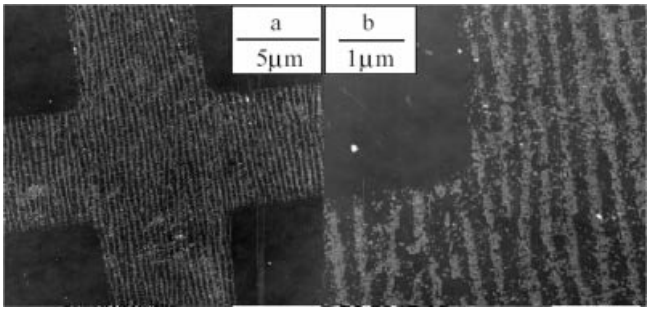

Figure 6. Topographic AFM images of $CdS/G8NH_2$ nanocomposites printed on an oxidised silicon wafer after two days ageing. A sub-micrometre stripe pattern develops inside the imposed cross-shaped pattern during the printing process.

While the structure formation is simple and straightforward, its physical interpretation is still unclear. An interesting question is whether the pattern is already present on the stamps. The inking process is the only chance for a mechanism based on fluid properties, such as dewetting. However, dewetting is excluded since it either results in structures confined to the borders of the printed pattern[47] or it yields foam-like structures in mobile molecular monolayers.[48] For some molecular systems, quite regular, but much larger, pattern widths (tens of micrometers) are found;[49,50] they depend on the orientation of the molecules on the surface, which should not play a role at the low coverages in the system under consideration. Indeed, the stripes presented here do not have uniform widths, but they extend over the complete micropatterned area. Similar, but better ordered,

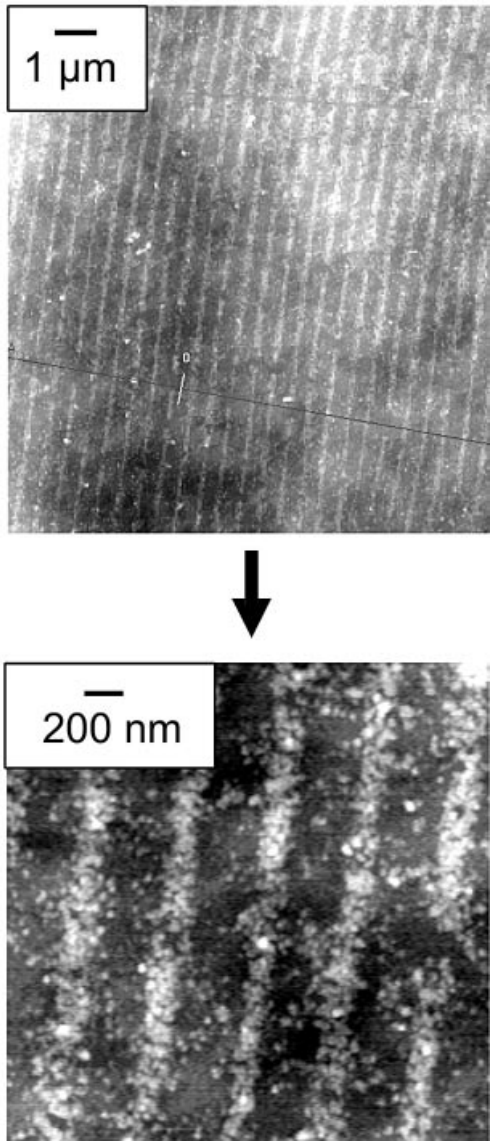

Figure 7. Topographic intermittent contact AFM image of CdS/$G8NH_2$ nanocomposites (aged for two days) printed on an oxidised silicon wafer with a flat stamp.

structures (linear arrays with sub-micrometer widths and a regular spacing) can be formed by dynamic monolayer film instabilities.[51] On the other hand, the composite does not form a complete monolayer, and the large CdS/dendrimer structures are not in all respects comparable with small molecules.

Another interesting point is the huge difference in behaviour between aged and fresh composites. This difference is unlikely to be chemical since both have chemical properties that are similar to pure dendrimers (see above). A clear difference is the (average) mass of the particles, which is relatively low for the fresh composites. However, possible mass-based mechanisms are hard to identify. For example, the stripe formation might suggest buckling, as observed upon heating, oxidation and cooling of PDMS,[52] or a standing wave, although a single acoustic resonance with a micrometre wavelength is unlikely.

2. Orientation of Plant Virions on Surfaces and the Synthesis of Metal Wires in Virions

When one-dimensional nanostructures or linear alignments of clusters are required, several supramolecular biotemplates can be advantageously employed for elegant syntheses (see Introduction). A good template for inorganic nanostructures is the tobacco mosaic virus (TMV). TMV is a tube-like assembly made up from around 2130 identical coat proteins helically organised around a helical single-strand RNA. Its length is about 300 nm and the outer diameter is 18 nm.[53] TMV has an inner channel with a diameter of 4 nm that is clad by the coat proteins. The interior of the channel is thus shielded from the environment; uranyl and most other cations cannot penetrate through the coat, and they have to diffuse in from either end.[26] TMVs are physically and chemically unusually stable − they can be suspended in several polar solvents (e.g. acetone and ethanol) without substantial changes of their structural integrity − and they tend to organise linearly in a head-to-tail fashion; in this way, the channel can be elongated to multiples of 300 nm.[28] Nanostructures can be created on the outer surface or in the interior channel.[28] The first case is analogous to nanostructures on other biomolecules such as DNA, whereas the second case is confinement templating, which has been documented for relatively few cases, for example peptide tubuli,[21] carbon nanotubes[54] and mesoporous silica.[55]

The nature of the coat proteins and the charges (TMV is negatively charged above its pI of 3.5) imply hydrophilicity and hydrogen-bonding capability, hence surfaces such as mica and oxidised silicon wafers are suitable for immobilisation. Due to the adsorption, TMV suffers some compression normal to the substrate surface.[28,56] Note that the adsorption on TEM grids is facile, too, since the standard carbon-coated polymer substrates are at least partially hydrophilic, much different from hydrophobic surfaces such as pure graphite or several polymers. Starting from this point, Section 2.1 investigates how to impose directional order, similar to the CdS/dendrimer stripes presented in Section 1.2.2, to adsorbed or adsorbing virions. Section 2.2 focuses on synthesising clusters and wires on and in a single TMV, so that the clusters are aligned by the linear biotemplate. This is obviously impossible with syntheses in near-spherical templates such as the dendrimers of Section 1.1.

2.1. Organising Tobacco Mosaic Virions in a Parallel Fashion by Lateral Forces

When oriented, but not necessarily patterned, assemblies of biomolecules are required, the simple application of directional mechanical forces during adsorption can be helpful. This method is well known for DNA,[9,29] but less so for much shorter (sub-micrometre) supramolecular units such as TMV. While TMV can organise in liquid-crystalline form at high concentrations, separate single virions form a statistically oriented assembly during adsorption to a substrate. Here it is demonstrated that single TMVs can be

aligned by applying shear forces during adsorption on a flat substrate surface.

The first approach relies on forces exerted by a directional gas stream (during drying of a droplet) or by a directional flow of solvent (during suction drying of a droplet) (Figure 8). An Mg^{2+}-treated mica surface was covered with a droplet of TMV suspension (0.1 mg/ml), and a stream of argon was directed at it to remove the supernatant. Figure 9 (a) shows the mica surface with aligned adsorbed single virions. Note that the alignment is not perfect (the relative angle between the viral axes is not zero); on the other hand, nearly all virions on a given substrate were found to be oriented. Many virions aggregate linearly, i.e. they organise into objects about 18 nm wide (due to tip convolution effects not detectable by AFM) and hundreds of nanometres long. The pressure of the gas stream has to exceed a certain value ($\approx$ 7 bar); alignment with lower argon pressure was never observed. In a related experiment, a droplet of TMV suspension was placed on a hydrophobic flat PDMS surface and exposed to the argon stream. The aligned virions on the PDMS surface were transferred to an oxidised silicon wafer surface by microcontact printing (Figure 8, b) and visualised by AFM. The results were nearly identical to those shown in Figure 9 (a).

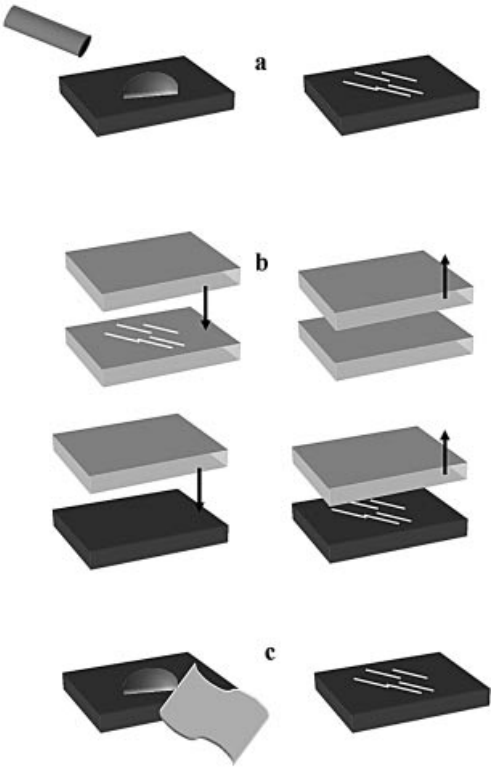

Figure 8. Orientation of nano-objects during their immobilisation by shear forces: (a) drying a droplet with a strong gas stream; (b) transfer of the oriented, adsorbed objects from PDMS to an oxidised wafer by microcontact printing with a flat PDMS stamp (top, arrows); (c) drying a droplet by suction with a filter paper.

An interpretation of this (top-down) process can be based on the initial attachment of only one end of the virion, since this is statistically much more likely than immediate contact of the complete virion. The virion is then free to rotate around the pivotal point for some time before it comes into contact with the substrate over its complete length. At this stage, lateral forces can act to orient the TMVs before they come into complete contact (Figure 8). The orientation is thereafter fixed, since the mobility of adsorbed TMV, especially on hydrophilic substrates, is very low. The alignment should, in both cases, be due to shear forces in the droplet, and it occurs during the diffusion to the surface. It is very unlikely that TMV, which adsorbs strongly on mica or silicon wafers, shows surface diffusion, which was never observed in any AFM experiment on mica or wafers or even graphite. A test verified that once a virion is adsorbed, it cannot reorient: placing a droplet of pure water on a surface coated with randomly adsorbed TMV, and thereafter subjecting it to an argon stream, did not produce aligned virions.

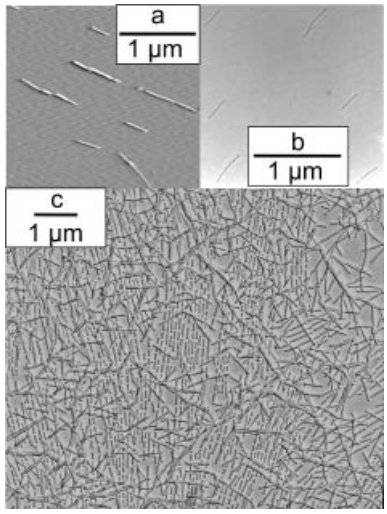

Figure 9. (a) AFM image (error signal) of TMV aligned by drying a droplet with an argon stream during adsorption on Mg^{2+}-treated mica. (b) Transmission electron micrograph (200 kV) of TMVs aligned by lateral forces (suction with filter paper) during adsorption on the carbon-coated polymer surface of a microscopy grid. No uranyl or other stain was applied. (c) as (b), but with higher TMV concentration and with silver shadowing to enhance the contrast (60 kV).

Coverage and orientation are not arbitrary, but in line with expectations: a droplet (max. 0.1 mL) with 0.1 mg mL^{-1} TMV provides sufficient material to deposit about eight monolayers of densely packed TMVs on the employed 1 cm^2 samples. However, coverages of only a tiny fraction of a monolayer were found. The typical diffusion time in the droplet to the surface is in the range of 1 h (for a droplet spread to 1 cm^2), while the droplet contact time was only 1 min, which should result in submonolayer coverage, as observed. In addition, in some cases (e.g. for graphite substrates or for the case of the hydrophobic stamp) a kinetic barrier due to colloid chemical effects can be present.[56] After the droplet contact time, the orienting force was applied; one can assume that the majority of the adsorbed virions are at this time contacting the surface with only one end. The gas stream exerts a force in the nanonew-

ton range: 7 bar acting on a 300 nm long and 18 nm wide area. This macroscopic force estimate is in line with forces required for (microscopic) AFM manipulation of TMV.[57]

Another promising possibility to align TMVs on a surface is to make use of laterally applied capillary forces, as is also possible for DNA[9] and carbon nanotubes.[58] A TMV suspension (20 μL, 10 mg mL^{-1}) was placed on a transmission electron microscope grid for 1 min, after which the droplet was removed by touching a filter paper to one side of the grid. The shrinking droplet caused a directional flow from the grid to the paper. Again, virions aligned in the direction of the flow, as shown in Figure 9 (see parts b and c). The difference between the figures is based on the much higher concentration of the suspension used for Figure 9 (c). Again, the objects more than 300 nm long are linearly aggregated TMVs. This alignment method, however, is only applicable for surfaces that show relatively weak interaction forces with the virions, such as carbon-coated TEM grids.[56]

In summary, the alignment of TMVs on surfaces can be obtained in several very simple ways based on lateral forces that act on a droplet of TMV suspension, which is, in turn, in contact with a substrate surface.

2.2. Clusters in Virions: Electroless Deposition

Metal clusters can be produced "bottom-up" with electroless deposition on, and also inside, TMV. The advantage of deposition inside the TMV channel is the inherent alignment of the clusters parallel to the viral axis. Here, only the initial and intermediate stages of the process are investigated. The first step is a sensitisation of the suspended virions with sub-2 nm Pd or Pt clusters (sources are Pd and Pt salts in aqueous solution). The clusters are, in fact, so small that identification of single clusters by (conventional) TEM is not possible; rather, the virions appear grey due to the presence of the clusters.[28] After removal of surplus metal ions, the suspension was mixed with a bath that contains the metal ion to be deposited (e.g. Ni^{II}) and a reductant (e.g. hypophosphite or dimethylamine borane, DMAB). The electron transfer from the reductant to the ion is catalysed by the Pd (or Pt) clusters, hence the deposition is limited to the location of the clusters. The deposition is autocatalytic, hence metal is continuously deposited on growing metal clusters. A side reaction is the evolution of hydrogen. The reaction is stopped by adding inhibitors or by drying the suspension, for example for analysis on a TEM grid. An important question is how the growing clusters develop into wires, and this question is obviously linked to the initial phase of the electroless deposition process.

When the original virus suspension contains phosphate, the reaction is limited to the outer viral surface, and relatively large (>30 nm diameter; not shown) coalescing clusters are found. Small clusters (<5 nm diameter) can be obtained by adsorption of noble metal salts, followed by reduction or by "mild" electroless deposition with hypophosphite.[19,26] Whenever the central viral channel can be found (e.g. in a cluster-free region), it is empty, proving the high selectivity of the reaction. The presence of phosphate is thought to result in insoluble deposits of metal phosphates (Co or Ni); these deposits, together with the noble metal clusters, act as very effective nucleation centres for the deposition.

In the absence of phosphate, the selectivity for channel metallisation is high, resulting in the deposition of wires. The selectivity for the channel is not easily explained. Electrostatic and complex chemistry arguments may favour the channel-cladding functional groups;[19,26,28] however, the observation of relatively large (>5 nm) clusters detached from the virions could mean that clusters initially form on the viral coat, but are unable to attach as strongly as in the presence of insoluble metal phosphates (see above). The by-product hydrogen may additionally exert mechanical forces, resulting in this detachment. The production of 3–4-nm-wide wires solely by wet chemical means cannot be achieved by any other process; however, chemical vapour deposition inside carbon nanotubes[54] appears to be an alternative to using TMV, while complete arrays of similar wires can be formed in mesoporous silica.[55] Figure 10 refers to an experiment where TMV was sensitised with Pd and metallised with Ni (in a DMAB-containing bath, see Experimental Section), but the process was interrupted before the time required for wires longer than 200 nm.[28] The lower part of Figure 10 shows the same image with different contrast, and with the positions of the wires marked as black lines. A number of wires already have remarkable lengths (>100 nm). Note that once again the TMVs in Figure 10 are linearly aligned, but that each orifice of the channels is still accessible (white arrows) and thus allows for electrolyte supply inside the TMVs. Hence, all distinct regions (here four) between the orifices appear to be metallised independently from their neighbours, resulting here in four wires.

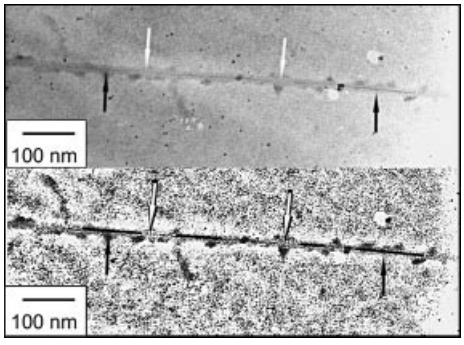

Figure 10. Transmission electron micrograph (200 kV) of Ni wires (<4 nm diameter) inside the TMV channel after electroless deposition in the absence of phosphate. Each gap between two virions is marked by white arrows and the wires by black arrows. The lower image is contrast-enhanced. The wires form upon nucleation and growth of Ni at sub-2 nm Pd clusters.

The mechanism is based on Pd or Pt nuclei that are rapidly covered by the metal (here Ni) that deposits from the electroless bath. Autocatalytic growth can result in depletion of reactive species and thus in size limitation.[59] However, the interior viral channel imposes a natural limit. Another limit is the solution concentration inside the channel: whenever two clusters have formed, a certain amount

of metal ions is trapped between them. This amount has a maximum of 400 atoms (0.18 M Ni^{II}, 300 nm length, 4 nm diameter), yielding a spherical cluster of less than 3 nm diameter. Hence, more than two clusters inside a single virion can only grow when the first cluster forms deep inside the channel, and the later ones step by step closer to the viral orifice, in line with observations.[19,26] The same argument explains why more than two wires are never found inside a single virion. Wires form when the reductant is DMAB, which is thermodynamically and kinetically superior to hypophosphite (which is used for cluster synthesis). This implies that of the large number of Pd or Pt nuclei, only a very few are highly active. These few clusters start a rapid process of filling the viral channel with the deposit (Figure 11).

Figure 11. Mechanism of electroless cluster and wire deposition inside a channel: (a) tube-like template (e.g. TMV); (b) sensitisation: formation of very small noble metal clusters on the exterior surface and on the interior walls; (c) initial deposition: only a few very active clusters grow fast, the clusters on the exterior surface detach; (d) the clusters inside the channel can grow to, at maximum, two wires per channel when metal ions are supplied from the orifices of the channel.

Conclusions

A simple, wet chemical precipitation process can be used for the "bottom-up" synthesis of semiconductor nanoclusters when dendrimer templates are present. To this end, a synthesis method that produces CdS clusters at the outer surface of poly(amidoamine) dendrimers was modified to yield clusters inside the dendrimers. Control of the pH during synthesis allows for selective protonation of some of the amine groups in the dendrimer; relevant Cd^{2+} binding processes have been identified. The charge of the template is a decisive factor in a successful synthesis and should be considered also in other cluster syntheses. Elegant "top-down" organisation/patterning of the CdS/dendrimer composites on surfaces can be attained with microcontact printing. In addition to simple patterns, sub-micrometre wide stripes, made up from adsorbed composites, develop during printing inside micrometre-sized patterns. Thus, microcontact printing can result in a surprising way (synchronously) in not only "top-down" but also "bottom-up" structuring.

Metal wires 3–4 nm in diameter can be obtained by electroless deposition from solutions containing metal ions and reductants. They grow in the central channels of plant virions; the earlier stages of this process have been analysed, and a mechanism for the selective deposition in the channels presented. Clearly, the method is capable of producing other high aspect structures in narrow tubes. Removal of the coat proteins should be possible by oxidative or enzymatic treatment.[21] Organisation of the virions on flat substrates can be achieved during adsorption by application of external forces to a suspension droplet, resulting in parallel alignment. This method is well known from adsorption studies of other linear biomolecules, but works well even for the relatively short virion length of 300 nm.

Experimental Section

Poly(amidoamine) (PAMAM) dendrimer (generation 8) terminated with amine (Dendritech, Inc., Midland), here referred to as $G8NH_2$, was dissolved in 99.8% ethanol (Roth) with concentrations from 0.5 μM to 50 μM. $G8NH_2$ (200 μL) was diluted with methanol to 10 mL (5.5 μM $G8NH_2$), then 10 mL of 2 mM $Cd(CH_3COO)_2$ and 10 mL of 0.7 mM Na_2S in methanol were added to the dendrimer solution sequentially. After reaction, the nanocomposites were stored in a freezer at –35 °C to reduce the Ostwald ripening growth of nanoparticles, or they were aged at 25 °C for two and 22 days to induce ripening. The final concentration of $G8NH_2$ in the solution was 1.83 μM. The Cd^{2+}/S^{2-} ratio was kept at 3:1 since it was found that at this ratio CdS/$G8NH_2$ nanocomposites could be successfully printed. Before adsorption and printing, nanocomposites were dialysed (Slide-A-Lyzer 10000 MWCO caps, KMF, Lohmar) against methanol. Experiments with generation 4 dendrimers were conducted in a similar manner.

Absorption spectra from solutions were obtained with a Perkin–Elmer UV/Vis spectrometer Lambda 2. Photoluminescence and excitation spectra were taken with a Perkin–Elmer luminescence spectrometer LS 50B. The solutions were placed in quartz cuvettes for both instruments.

Silicon wafers [orientation (100), Crystal, Berlin] were terminated by silicon oxide with hydroxyl groups by the standard RCA procedure: 15 min immersion in a 65–75 °C hot 1:1:5 mixture of 25% NH_4OH (VLSI Selectipur, Merck), 31% H_2O_2 (VLSI Selectipur, Merck) and water (Millipore, 18 MΩcm) followed by 15 min immersion in a 65–75 °C hot 1:1:5 mixture of 37% HCl (Suprapur, Merck), 31% H_2O_2 and water. These samples are termed "oxidised silicon wafers".

Ellipsometric measurements were performed in air with an EL-X-02C ellipsometer (DRE, Ratzeburg) at 70° angle of incidence and 633 nm wavelength. The ellipticity of the HeNe laser beam was minimised with a λ/4 plate. Measurements were made at more than 4 points randomly picked across the sample and averaged. A two-layer transparent film model was used for the thickness calculations of dendrimer layers on oxidised silicon wafers. The refractive index of the dendrimers was fixed at 1.45.

Atomic force microscope (AFM) images of patterns were obtained in intermittent contact mode with a Thermomicroscopes Autoprobe M5, operated in non-contact and intermittent contact mode, with MikroMasch NSC11 tips or NCHR Pointprobe Nanosensors.

Poly(dimethylsiloxane) (PDMS) stamps (Sylgard 184, Dow Corning) were formed on flat polystyrene dishes or on patterned silicon wafer masters [IBM Zürich and Institute for Microelectronics Stuttgart (IMS); before first use the master was rendered hydrophobic with fluoroalkyltrichlorosilane vapour]. The stamps were activated by plasma oxidation in 1 mbar O_2 at 150 mW for 10 s (Technics Plasma 100-E). Hydrophilicity was ensured by contact angle measurements for various exposure times from 0 s to more than 10 s. Freshly activated flat stamps were covered with one drop (≈20 μL) of ink solution for 25 s, and then blown dry with argon. Freshly activated structured stamps were brought into conformal

contact with the inked flat stamp for 25 s, then peeled off and brought into conformal contact with freshly cleaned silicon wafers for 25 s, and finally peeled off from the substrates.

For the TMV alignment, freshly cleaved mica was treated for 5–15 min with 0.1–1 M aqueous $MgCl_2$. The surface was contacted with a droplet of TMV suspension (0.1 mg mL^{-1}). After 1 min (known to be sufficient for strong adsorption) a strong stream of argon (7–8 bar, 5 mm orifice) was directed at about 65° to the surface normal to remove the supernatant. Alignment by laterally applied capillary forces was achieved as follows: A Formvar/carbon-coated copper grid (300 or 400 mesh, SPI-Supplies) was dipped into ethanol (Roth Rotipuran) and air-dried. TMV suspension (20 μL, 10 mg mL^{-1}) was placed on the grid. After 2–3 min the solution was removed by placing filter paper on one side of the grid. TEM images were obtained with a Philips CM200 at 200 kV and − in this case after silver shadowing − in a Zeiss EM 10 at 60 kV.

TMV was metallised in the following way: First, a TMV suspension (0.1–0.2 mg mL^{-1}) was mixed with an equal volume of a 0.9 mM solution of Na_2PdCl_4 or K_2PtCl_4 (both p.a., Aldrich) in 1 M NaCl (p.a., Fluka), adjusted to pH 5–6 with 0.1 M HCl. After an incubation time of 10 min, the suspension was centrifuged at 14000 rpm for 10 min and the supernatant carefully removed. The pellet was resuspended in water and centrifuged again for 10 min at 14000 rpm in order to remove remaining Pd or Pt. This washing procedure was applied 2–3 times. Ni was deposited from 0.18 M $Ni(CH_3COO)_2{\cdot}4H_2O$ (p.a., Fluka), 0.28 M lactic acid (85% in water, Fluka) and 34 mM DMAB (dimethylamine borane, p.a., Aldrich) in water. The pH was adjusted to 6–7 with 1 M NaOH solution. TEM images were obtained with a Philips CM200 at 200 kV.

[1] M. Möller, J. Spatz, *Curr. Opin. Colloid Interface Sci.* **1997**, *2*, 177–187.
[2] C. M. Niemeyer, *Angew. Chem. Int. Ed.* **2001**, *40*, 4128–4158.
[3] A. M. Bittner, *Naturwissenschaften* **2005**, *92*, 51–64.
[4] M. Pileni, *Cryst. Res. Technol.* **1998**, *33*, 1155–1186.
[5] H.-G. Boyen, K. Fauth, B. Stahl, P. Ziemann, G. Kästle, F. Weigl, F. Banhart, M. Hessler, G. Schütz, N. S. Gajbhiye, J. Ellrich, H. Hahn, M. Büttner, M. G. Garnier, P. Oelhafen, *Adv. Mater.* **2005**, *17*, 574–578.
[6] X. C. Wu, A. M. Bittner, K. Kern, *J. Phys. Chem. B* **2005**, *109*, 230–239.
[7] X. C. Wu, A. M. Bittner, K. Kern, *Adv. Mater.* **2004**, *16*, 413–417.
[8] M. Steigerwald, L. Brus, *Acc. Chem. Res.* **1990**, *23*, 183–188.
[9] H. Nakao, M. Gad, S. Sugiyama, K. Otobe, T. Ohtani, *J. Am. Chem. Soc.* **2003**, *125*, 7162–7163.
[10] Y. Sun, J. A. Rogers, *Nano Lett.* **2004**, *4*, 1953–1959.
[11] E. Strable, J. M. Bulte, B. Moskowitz, K. Vivekanandan, M. Allen, T. Douglas, *Chem. Mater.* **2001**, *13*, 2201–2209.
[12] M. Q. Zhao, R. M. Crooks, *Angew. Chem. Int. Ed.* **1999**, *38*, 364–366.
[13] J. Zheng, M. S. Stevenson, R. S. Hikida, P. V. Van Patten, *J. Phys. Chem. B* **2002**, *106*, 1252–1255.
[14] N. C. B. Tan, L. Balogh, S. F. Trevino, D. A. Tomalia, J. S. Lin, *Polymer* **1999**, *40*, 2537–2545.
[15] B. I. Lemon, R. M. Crooks, *J. Am. Chem. Soc.* **2000**, *122*, 12886–12887.
[16] J. J. J. M. Donners, R. Hoogenboom, A. P. H. J. Schenning, P. A. van Hal, R. J. M. Nolte, E. W. Meijer, N. A. J. Sommerdijk, *Langmuir* **2002**, *18*, 2571–2576.
[17] K. Sooklal, L. H. Hanus, H. J. Ploehn, C. J. Murphy, *Adv. Mater.* **1998**, *10*, 1083–1087.
[18] E. Braun, Y. Eichen, U. Sivan, G. Ben-Yoseph, *Nature* **1998**, *391*, 775–778.
[19] M. Knez, M. Sumser, A. M. Bittner, C. Wege, H. Jeske, T. P. Martin, K. Kern, *Adv. Funct. Mater.* **2004**, *14*, 116–124.
[20] C. E. Flynn, S.-W. Lee, B. R. Peelle, A. M. Belcher, *Acta Mater.* **2003**, *51*, 5867–5880.
[21] M. Reches, E. Gazit, *Science* **2003**, *300*, 625–627.
[22] S. Behrens, K. Rahn, W. Habicht, K.-J. Böhm, H. Rösner, E. Dinjus, E. Unger, *Adv. Mater.* **2002**, *14*, 1621–1625.
[23] M. Mertig, R. Kirsch, W. Pompe, *Appl. Phys. A* **1998**, *66*, S723–S727.
[24] T. Scheibel, R. Parthasarathy, G. Sawicki, X. M. Lin, H. Jaeger, S. L. Lindquist, *Proc. Natl. Acad. Sci. USA* **2003**, *100*, 4527–4532.
[25] J. Richter, M. Mertig, W. Pompe, I. Mönch, H. K. Schackert, *Appl. Phys. Lett.* **2001**, *78*, 536–538.
[26] E. Dujardin, C. Peet, G. Stubbs, J. N. Culver, S. Mann, *Nano Lett.* **2003**, *3*, 413–417.
[27] Q. Wang, T. Lin, L. Tang, J. E. Johnson, M. G. Finn, *Angew. Chem. Int. Ed.* **2002**, *41*, 477–480.
[28] M. Knez, A. M. Bittner, F. Boes, C. Wege, H. Jeske, E. Maiß, K. Kern, *Nano Lett.* **2003**, *3*, 1079–1082.
[29] Z. Deng, C. Mao, *Nano Lett.* **2003**, *3*, 1545–1548.
[30] H. Nakao, H. Shiigi, Y. Yamamoto, S. Tokonami, T. Nagaoka, S. Sugiyama, T. Ohtani, *Nano Lett.* **2003**, *3*, 1391–1394.
[31] R. C. van Duivenbode, M. Borkovec, G. J. M. Koper, *Polymer* **1998**, *39*, 2657–2664.
[32] L. Balogh, R. Valluzzi, K. S. Laverdure, S. P. Gido, G. L. Hagnauer, D. A. Tomalia, *J. Nanopart. Res.* **1999**, *1*, 353–368.
[33] F. Gröhn, B. J. Bauer, Y. A. Akpalu, C. L. Jackson, E. J. Amis, *Macromolecules* **2000**, *33*, 6042–6050.
[34] S. V. Gaponenko, *Optical Properties of Semiconductor Nanocrystals*, Cambridge University Press, **1998**, p. 53.
[35] L. Balogh, D. A. Tomalia, *J. Am. Chem. Soc.* **1998**, *120*, 7355–7356.
[36] M. Q. Zhao, R. M. Crooks, *J. Am. Chem. Soc.* **1998**, *120*, 4877–4878.
[37] G. J. M. Koper, M. H. P. van Genderen, C. Elissen-Roman, M. W. P. L. Baars, E. W. Meijer, M. Borkovec, *J. Am. Chem. Soc.* **1997**, *119*, 6512–6521.
[38] G. G. Guilbault, S. M. Billedeau, *J. Inorg. Nucl. Chem.* **1972**, *34*, 1167.
[39] M. F. Ottaviani, F. Montalti, N. J. Turro, D. A. Tomalia, *J. Phys. Chem. B* **1997**, *101*, 158–166.
[40] E. Delamarche, H. Schmid, A. Bietsch, N. B. Larsen, H. Rothuizen, B. Michel, H. Biebuyck, *J. Phys. Chem. B* **1998**, *102*, 3324–3334.
[41] K. Kuhnke, D. M. P. Hoffmann, X. C. Wu, A. M. Bittner, K. Kern, *Appl. Phys. Lett.* **2003**, *83*, 3830–3832.
[42] N. Lu, X. Chen, D. Molenda, A. Naber, H. Fuchs, D. V. Talapin, H. Weller, J. Müller, J. M. Lupton, J. Feldmann, A. L. Rogach, L. F. Chi, *Nano Lett.* **2004**, *4*, 885–888.
[43] A. M. Bittner, X. C. Wu, K. Kern, *Adv. Funct. Mater.* **2002**, *12*, 432–436.
[44] J. Li, L. T. Piehler, J. R. Baker, D. A. Tomalia, *Langmuir* **2000**, *16*, 5613–5616.
[45] V. V. Tsukruk, F. Rinderspacher, V. N. Bliznyuk, *Langmuir* **1997**, *13*, 2171–2176.
[46] X. C. Wu, A. M. Bittner, K. Kern, *Langmuir* **2002**, *18*, 4984–4988.
[47] Y. Xia, D. Qin, Y. Yin, *Curr. Opin. Colloid Interface Sci.* **2001**, *6*, 54–64.
[48] K. J. Stine, C. M. Knobler, *Phys. Rev. Lett.* **1990**, *65*, 1004–1007.
[49] D. K. Schwartz, J. Ruiz-Garcia, X. Qiu, J. V. Selinger, C. M. Knobler, *Physica A* **1994**, *204*, 606–615.
[50] H. Choi, X. Yang, G. W. Mitchell, C. P. Collier, F. Wudl, J. R. Heath, *J. Phys. Chem. B* **2002**, *106*, 1833–1839.
[51] M. Gleiche, L. F. Chi, H. Fuchs, *Nature* **2000**, *403*, 173–175.
[52] N. Bowden, W. T. S. Huck, K. E. Paul, G. Whitesides, *Appl. Phys. Lett.* **1999**, *75*, 2557–2559.
[53] M. Zaitlin, *AAB Descriptions of Plant Viruses* **2000**, *370*, 8.

[54] B. K. Pradhan, T. Kyotani, A. Tomita, *Chem. Commun.* **1999**, 1317–1318.
[55] O. Kazakova, D. Erts, T. A. Crowley, J. S. Kulkarni, J. D. Holmes, *J. Magn. Magn. Mater.* **2005**, *286*, 171–176.
[56] M. Knez, M. P. Sumser, A. M. Bittner, C. Wege, H. Jeske, D. M. P. Hoffmann, K. Kuhnke, K. Kern, *Langmuir* **2004**, *20*, 441–447.
[57] M. R. Falvo, S. Washburn, R. Superfine, M. Finch, F. P. Brooks, Jr., V. Chi, R. M. Taylor II, *Biophys. J.* **1997**, *72*, 1396–1403.
[58] Y. Huang, X. Duan, Q. Wei, C. M. Lieber, *Science* **2001**, *291*, 630–633.
[59] H. Kind, A. M. Bittner, O. Cavalleri, K. Kern, T. Greber, *J. Phys. Chem. B* **1998**, *102*, 7582–7589.

Received: April 30, 2005
Published Online: August 17, 2005

